On the application of the method of finite spheres to problems in tribology

Michael Macri — John Tichy — Suvranu De

Department of Mechanical
Aerospace and Nuclear Engineering
Rensselaer Polytechnic Institute
Troy, NY 12180, USA

ABSTRACT. *In this paper we introduce the method of finite spheres, a truly meshfree numerical technique, as a promising scheme for the solution of problems arising in tribology. Some of the attractive features of this technique, contrasted to the traditional finite element methods, include the use of smooth approximation spaces which can be enriched using known asymptotic solutions of the governing partial differential equations as well as the freedom from generation of a complex computational mesh and the need for remeshing for problems involving very large deformations or changes in topology. An elastostatic punch indentation problem is used to showcase the various positive attributes of this method.*

RESUME. *Dans cet article nous présentons la méthode de sphères finies, une véritable technique numérique de « maillage libre », comme schéma prometteur pour la solution de problèmes tribologiques. Certains aspects attrayants de cette technique, contrairement aux méthodes d'élément finis traditionnelles, incluent l'utilisation d'espaces d'approximation qui peuvent être enrichis en utilisant des solutions asymptotiques connues d'équations aux dérivées partielles ainsi que l'absence de la génération de maillages complexes et le besoin de remaillage des problèmes impliquant des grandes déformations ou des changements importants de topologie. Un problème élastostatique d'indentation de poinçon est traité pour présenter les divers aspects positifs de cette méthode.*

MOTS-CLES : *méthode de sphères finies, indentation, tribologie, enrichissement.*

KEYWORDS. *meshless methods, method of finite spheres, indentation, tribology, enrichment.*

REEF – 14/2005. Finite elements in tribology, pages 339 to 366

1. Introduction

Tribology (the study of interacting surfaces in relative motion) is, by its nature, an interdisciplinary field, if the reader will pardon the cliché. However, in using the term "tribology", if we restrict ourselves to mechanical aspects, we can loosely divide the field into domains governed by the mechanics of solids (the bodies that form the surfaces) and the mechanics of fluids (the lubricants confined between the surfaces). In many cases there is a coupling between fluid and solid behavior (elastohydrodynamics).

Although the definition is not always strictly obeyed, the term contact mechanics is applied to the case when the region of contact is much smaller than the dimensions of the body as a whole, such that stresses in the contact region are independent of the size and shape of the body. This situation generally occurs in non-conformal contacts when bodies would first touch at a point or along a line.

Finite element techniques (Bathe, 1996) are certainly commonplace in the field of tribology. In these techniques the continuum is discretized using "elements" which are connected together at special points called "nodes" (figure 1a). The technique of discretizing a continuum by elements is known as "mesh generation".

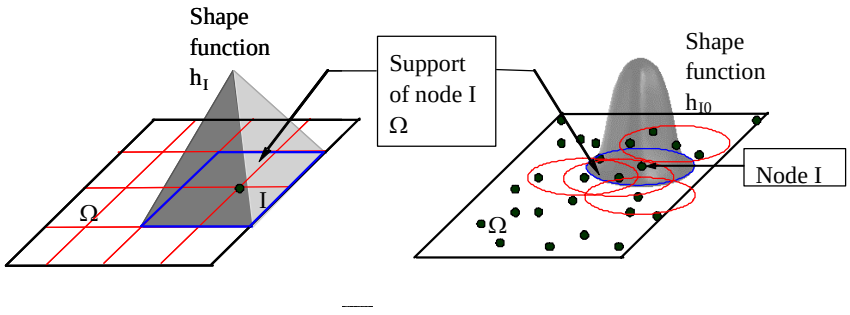

(a) Finite element method (b) Method of finite spheres

Figure 1. *Discretization of a domain, $\Omega \in R^2$, by the finite element method (a) and the method of finite spheres (b). In (a), the domain is discretized by quadrilateral elements with a node at each vertex point. The finite element shape function h_I is shown at node I. In (b), the domain is discretized using a set of nodes only. Corresponding to each node I, there is a sphere (i.e. a disk in R^2), centered at the node, which is the support of a set of shape functions corresponding to that node. One such shape function, h_{I0}, is shown in the figure*

From an unscientific survey of a year of issues of the ASME *Journal of Tribology*, it appears that about one quarter to one third of the non-experimental papers use *finite* element techniques in one form or another. In the case of fluid flow

analysis, finite elements are used to model the complex grooves of seal geometry (Ruan, 2000; Baheti *et al.*, 1995) and the moving or unknown boundaries of cavitation problems (Optasanu *et al.*, 2000). In the analysis of solids, non-conformal problems are typically considered in the case of rolling contacts (Xu *et al.*, 2002), indentations (Stephens *et al.*, 2000), and rough surface contact simulations (Jacq *et al.*, 2002; Komvopoulos *et al.*, 2002) (often as layered media). Conformal contacts are studied in such applications as brakes (Geijselaers *et al.*, 2000) and chemical mechanical polishing (Kim *et al.*, 2003). This is by no means meant to be a comprehensive survey, but rather to give the reader some idea as to the nature of the existing literature.

In many ways, finite element analysis is not particularly well-suited to tribology problems. The strength of the finite element method is in accommodating complex geometry, but in many regards tribology geometries are relatively simple (journal bearing eccentric cylinder shapes, sphere-on-flat, triangular indenter, etc.). The complexities are due to unknown boundary shapes (*e.g.*, in the case of non-conformal contacts), and due to the existence of singularity-like behavior at the shape edges of indentation contacts, as in (Stephens *et al.*, 2000; Geijselaers *et al.*, 2000; Kim *et al.*, 2003). In this paper we focus on the latter issue – sharp edges and singularities.

The solution in the vicinity of a singularity is poorly approximated by polynomials, which are used in traditional finite element methods unless a very refined mesh is utilized. In such cases it is expedient to exploit the structure of the underlying differential equations to generate enriched approximation spaces to achieve accelerated convergence rates. In the context of the finite element method, for instance, special elements such as quarter-point elements (Banks-Sills *et al.*, 1984; Barsoum, 1984) and enriched elements (Akin, 1976) have been developed to generate non-polynomial approximation spaces. However, the schemes lack generality, as it is possible to generate only a limited number of such non-polynomial approximations.

Another major problem of the traditional finite element schemes is associated with the generation of a "good quality" mesh. The finite elements need to satisfy certain stringent conditions on the aspect ratios of sides and included angles, which make the automatic generation of a good quality mesh a nontrivial task, especially in three-dimensions. Furthermore, expensive remeshing is required for problems that involve topology changes, such as dynamic crack propagation.

In the finite element techniques, the mesh is generated to define the shape functions, which are piece-wise Lagrange polynomials. Hence the displacement approximation is usually C^0. For problems with singularities, the lack of continuity of the stress field across the elements results in poor convergence rates (Bathe, 1996).

To alleviate these problems associated with the traditional finite element schemes, we introduced the method of finite spheres (De *et al.*, 2001). In this

method the discretization is performed using functions that are compactly supported on n-dimensional spheres centered at nodal points, see figure 1b. The compact support of the functions results in banded stiffness matrices just as in the finite element methods. However, since the supports of the shape functions are regular, the element Jacobians are well behaved. The only important criterion that needs to be satisfied is that the union of the spheres must cover the entire domain. Therefore, generating an acceptable nodal arrangement in the method of finite spheres is not as difficult as generating a good quality mesh for a traditional finite element analysis. This is a definite advantage for many problems in the linear and nonlinear analysis of solids and structures and fluid-structure systems.

The method of finite spheres may be viewed as a generalized finite element technique in which the spheres behave conceptually as finite elements. However, unlike the traditional finite elements, the spheres are not constrained to abut each other.

One of the major advantages of this technique is that it is rather straightforward to generate approximation spaces having higher order continuity. Hence stresses are continuous over the entire domain and no special smoothening algorithms are required as in the finite element methods. Enhanced stress continuity reflects in higher convergence rates in problems having singularities as has been shown in (De *et al.*, 2001). Additionally, as we demonstrate in this paper, approximation spaces may be easily enriched with known asymptotic solutions of the governing partial differential equations in the vicinity of singularities such that the computed solution converges rapidly to the analytical solution of the mathematical model.

Over the past decade quite a few meshfree techniques have been proposed including the smoothed particle hydrodynamics (SPH) method (Monaghan, 1988), the diffuse element method (DEM) (Nayroles *et al.*, 1992), the element free Galerkin (EFG) method (Belytschko *et al.*, 1994), the reproducing kernel particle method (RKPM) (Liu *et al.*, 1993), the moving least-squares reproducing kernel method (MLSRK) (Li *et al.*, 1996), the partition of unity finite element method (PUFEM) ((Melenk *et al.*, 1996; Babuska *et al.*, 1997)), the *hp*-clouds method (Duarte *et al.*, 1996), the reproducing kernel hierarchical partition of unity method ((Li *et al.*, 1999)), the finite point method (Onate *et al.*, 1996), the local boundary integral equation (LBIE) method (Zhu *et al.*, 1998) and the meshless local Petrov-Galerkin (MLPG) method (Atluri *et al.*, 1998).

However, the majority of these techniques, such as the element free Galerkin and *hp*-clouds methods, are “pseudo meshfree” since only the approximation functions are generated in a meshfree manner, but a background mesh is required for the purpose of numerical integration of the terms arising in the Galerkin weak form. Moreover, little attention has been paid to develop a computationally efficient meshfree numerical method. While meshfree methods are attractive, if they are not efficient compared to traditional finite element methods, there is little hope of developing them as practical computational tools for general use.

The method of finite spheres, on the other hand, is a "truly meshfree" method since both interpolation and numerical integration are carried out without any background mesh. Moreover, in this method, the computational sub-domains, the interpolation functions, techniques of applying boundary conditions and performing numerical integration have been chosen with the issue of computational efficiency in mind. In (Macri *et al.*, 2004) we have reported that, for problems in 2D elastostatics, the method is now comparable in speed with traditional finite element methods, a feat which is not shared by any existing Galerkin-based meshfree method.

In this paper we discuss the advantages of using the method of finite spheres for problems in tribology with special reference to a problem of punch indentation and demonstrate that the use of smooth approximation spaces with enrichment does indeed result in superior solutions compared to finite elements with much coarser discretization.

In section 2 we briefly introduce the method of finite spheres with special emphasis on certain properties that govern the behavior of the method when enrichments are applied to the displacement fields. In section 3 we investigate the traditional problem of a square-sided rigid flat punch indenting a linear-elastic half-space and develop enriched approximation spaces. Finally, in section 4 we apply the method of finite spheres with enrichment to the solution of a problem involving the indentation of a two-dimensional linear elastic block, in plane strain, by a square-sided rigid flat punch and compare the solution with that obtained using the traditional finite element methods. Both frictionless and no slip conditions are considered.

2. Introduction to the Method of Finite Spheres

In the method of finite spheres the computational domain, Ω, is covered by overlapping and intersecting spheres centered at nodal points (figure 2a). Let $\left\{B\left(\mathbf{x}_I, r_I\right);\ \text{I=1,2,...,N}\right\}$ be a set of open spheres, where $\mathbf{x}_I$ and r_I refer to the centroid and radius of sphere '*I* ', respectively, such that $\Omega \subset \bigcup_{I=1}^{N} B(\mathbf{x}_I, r_I)$. The boundary of the sphere at node '*I* 'is denoted by $S\left(\mathbf{x}_I, r_I\right)$. First we discuss the generation of the approximation functions and their salient properties in section 2.1, followed by their application, in a Galerkin framework, to problems in linear elastostatics.

2.1. *The approximation scheme and general enrichment techniques*

In the method of finite spheres we generate shape functions using the partition of unity paradigm (Li *et al.*, 1999) based on the Shepard partition of unity functions (Shepard, 1968). The first step of this process is to define, at each node '*I* ', a

weighting function W_I that is compactly supported on the sphere at node '*I*' and has the following properties:

1) $W_I(\mathbf{x}) \in C_0^s\left(\overline{B}(\mathbf{x}_I, r_I)\right)$, $\quad s \geq 0$

2) $W_I(\mathbf{x}) \geq 0 \quad \forall \mathbf{x} \in \overline{B}(\mathbf{x}_I, r_I)$

3) $W_I(\mathbf{x}) = 0 \quad$ elsewhere

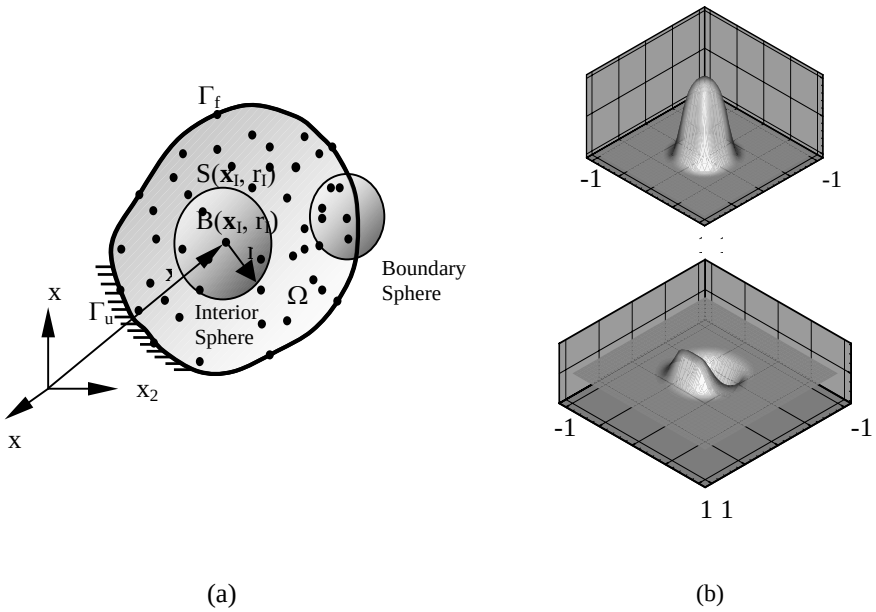

(a) (b)

Figure 2. *(a) A schematic of the method of finite spheres and (b) some shape functions in two-dimensions*

The symbol $C_0^s\left(\overline{B}(\mathbf{x}_I, r_I)\right)$ stands for the space of functions that are compactly supported on $\overline{B}(\mathbf{x}_I, r_I) = B(\mathbf{x}_I, r_I) \cup S(\mathbf{x}_I, r_I)$ which have continuous derivates of order '*s*'. With an abuse of notation we will choose W(**x**) = W(s_I) where $s_I = \|\mathbf{x} - \mathbf{x}_I\|_0 / r_I$, where $\|\bullet\|_0$ denotes the usual Euclidian norm. In our work we have chosen radial quartic spline weighting functions of the form:

$$W(s_I) = \begin{cases} 1 - 6s_I^2 + 8s_I^3 - 3s_I^4, & s_I \leq 1 \\ 0, & s_I > 1 \end{cases} \qquad [2.1]$$

Using these weighting functions, we define the Shepard partition of unity function (Shepard, 1968) at each node '*I'*, by a simple normalization procedure as:

$$\phi_I^0 = \frac{W_I}{\sum_{J=1}^{N} W_J} \quad \text{I=1,2,...,N} \tag{2.2}$$

The interesting properties of these functions are:

1. Partition of unity property: $\sum_{I=1}^{N} \phi_I^0(\mathbf{x}) = 1 \qquad \forall \mathbf{x} \in \Omega$

2. Continuity: $\phi_I^0(\mathbf{x}) \in C_0^s(R^d), \quad s \geq 0; d \in \{1,2,3\}$

From the partition of unity property it follows that the functions $\left\{\phi_I^0(\mathbf{x})\right\}$ satisfy zeroth order consistency, *i.e.* they ensure that rigid body modes are exactly satisfied. However, to be able to solve the elasticity equations, we need at least a first order consistent scheme that ensures constant strain states. The partition of unity paradigm provides a very general route to generating approximation spaces with higher order reproducing conditions, of which higher order consistency is a special case. We will first describe the general technique followed by special examples.

We define, at each node '*I'*, a local approximation space

$$V_I^{h,p} = span_{m\in\zeta}\left\{p_m(\mathbf{x})\right\} \subset H^1\left(B(\mathbf{x}_I, r_I) \cap \Omega\right) \tag{2.3}$$

where '*h*' is a measure of the size of the spheres, '*p*' is the polynomial order, ζ is an index set, $p_m(\mathbf{x})$ is a polynomial or other function and H^1 is the first order Hilbert space.

The global approximation space, $V^{h,p}$, is generated by pasting together the local approximation spaces using the Shepard functions as shown below:

$$V^{h,p} = \sum_{I=1}^{N} \phi_I^0 V_I^{h,p} \subset H^1(\Omega) \tag{2.4}$$

Hence, any function, $v^{h,p} \in V^{h,p}$ can be written as

$$v^{h,p}(\mathbf{x}) = \sum_{I=1}^{N} \sum_{m\in\zeta} h_{\mathrm{Im}}(\mathbf{x}) \alpha_{\mathrm{Im}} \tag{2.5}$$

where

$$h_{\mathrm{Im}}(\mathbf{x}) = \phi_I^0(\mathbf{x}) p_m(\mathbf{x}) \tag{2.6}$$

is the shape function at node '*I* ' corresponding to the m^{th} degree of freedom. In the method of finite spheres there are, therefore, multiple shape functions per node in contrast to the finite element method where there is just one shape function per finite element node. Figure 2b shows several shape functions generated at a node on a two-dimensional domain.

We see that if any function $p_n(\mathbf{x})$ is included in the local basis of each and every node then, choosing $\alpha_{\mathrm{Im}} = \delta_{mn} \forall I$ (where δ_{mn} is the Kronecker delta) in equation [2.5] and using [2.6] and the partition of unity property

$$\sum_{I=1}^{N} \sum_{m \in \zeta} h_{\mathrm{Im}}(\mathbf{x}) \alpha_{\mathrm{Im}} = p_n(\mathbf{x}) \left(\sum_{I=1}^{N} \phi_I^0(\mathbf{x}) \right) = p_n(\mathbf{x}) \qquad [2.7]$$

Hence it is possible to exactly reproduce the function over the entire domain. This is the **reproducing condition** of the shape functions.

Choosing the functions in the local basis as polynomials, for example, it is possible to generate approximation schemes which have higher order consistency. For instance, if $V_I^{h,p} = span\{1, x, y\}$ then a linearly accurate scheme, much like linear finite elements, is achieved in 2D. Choosing $V_I^{h,p} = span\{1, x, y, x^2, xy, y^2\}$, on the other hand, results in quadratic completeness. To prevent ill conditioning, we scale the basis polynomials, *e.g.*, we choose $V_I^{h,p} = span\{1, (x - x_I)/r_I, (y - y_I)/r_I\}$ instead of $V_I^{h,p} = span\{1, x, y\}$.

However, one is not limited in the choice of the enrichment functions $p_n(\mathbf{x})$ to just polynomials. The reproducing property of the approximation functions allows us great flexibility to generate approximation spaces that can embed known asymptotic solutions of the governing partial differential equations. We state (without proof) the following theorem, which demonstrates the effectiveness of the enrichment process:

***Theorem (A priori approximation error estimate)*:** *Let u be the function to be approximated, such that* $u \in H^k(\Omega), k \geq 2$ *and let* $\{\phi^0(\mathbf{x})\}$ *satisfy the conditions:*

1. $\left\| \phi_I^0 \right\|_{L^\infty(R^n)} \leq C$

2. $\left\| \nabla \phi_I^0 \right\|_{L^\infty(R^n)} \leq \dfrac{C}{r_I}$

Assume that the local approximation $V_I^{h,p}$ *has the following properties: on each* $\left(B(\mathbf{x}_I, r_I) \cap \Omega \right)$, *u can be approximated by the function* $v_I^{h,p} \in V_I^{h,p}$, *such that*

$$\begin{aligned}\left\|u-v_I^{h,p}\right\|_{L^2\left(B(\mathbf{x}_I,r_I)\cap\Omega\right)} &\le \varepsilon_1\left(I,h,p,u\right)\\ \left\|\nabla\left(u-v_I^{h,p}\right)\right\|_{L^2\left(B(\mathbf{x}_I,r_I)\cap\Omega\right)} &\le \varepsilon_2\left(I,h,p,u\right)\end{aligned} \qquad [2.8]$$

then there is a function $v^{h,p}\in V^{h,p}$ *satisfying*:

$$\begin{aligned}\left\|u-v^{h,p}\right\|_{L^2(\Omega)} &\le C\left(\sum_{I=1}^{N}\left(\varepsilon_1\left(I,h,p,u\right)\right)^2\right)^{1/2}\\ \left\|\nabla\left(u-v^{h,p}\right)\right\|_{L^2(\Omega)} &\le \left(\sum_{I=1}^{N}\left(\frac{C}{r_I}\right)^2\left(\varepsilon_1\left(I,h,p,u\right)\right)^2+C\left(\varepsilon_2\left(I,h,p,u\right)\right)^2\right)^{1/2}\end{aligned} \qquad [2.9]$$

where the symbol C denotes a positive generic constant which may take different values at successive occurrences.

Unlike moving least squares techniques, the partition of unity paradigm allows the enrichment to be varied from node to node. In section 3 we show the construction of specialized enrichment functions to solve a specific problem.

Another remarkable property of the shape functions (2.6) in the method of finite spheres is that they satisfy $h_{\mathrm{lm}}\left(x\right)\in C_0^{\min(s,l)}\left(\Omega_I\bigcap\Omega\right)$ where $W_I,\ I=1,2,...,N\ \in\ C_0^s\left(\Omega_I\right)$ and $p_m\left(\mathbf{x}\right)\in C^l\left(\Omega\right)$ for $s,l\ge 0$. Hence, by essentially choosing smooth weighting functions, it is possible to develop global approximation spaces on complex domains which inherit the smoothness of the weighting functions. This property of global smoothness is unique to this technique and is in sharp contrast to piece-wise continuous approximation spaces used in the finite element methods.

2.2. The discretization of linear elastic problems in R^2 using the method of finite spheres

In this section we present an example of how the approximation schemes developed in the previous section may be used to solve linear elastostatic problems in R^2. The system of governing equations can be written as:

Equilibrium equations:

$$\partial_\varepsilon^T\boldsymbol{\sigma}+\mathbf{f}^B=\mathbf{0}\quad\text{in }\Omega \qquad [2.10]$$

Strain-displacement relationship:

$$\boldsymbol{\varepsilon} = \partial_{\varepsilon}\mathbf{u} \quad \text{in } \Omega \tag{2.11}$$

Linear elastic constitutive equations

$$\boldsymbol{\sigma} = \mathbf{C}\boldsymbol{\varepsilon} \quad \text{in } \Omega \tag{2.12}$$

Boundary Conditions

$$\mathbf{N}\boldsymbol{\sigma} = \mathbf{f}^{s} \quad \text{on } \Gamma_{f} \tag{2.13}$$

$$\mathbf{u} = \mathbf{u}^{s} \quad \text{on } \Gamma_{u} \tag{2.14}$$

In the equation [2.10] to [2.14], **u**, **ε** and **σ** are, respectively, the displacement, stress and strain vectors, **C** is the elasticity matrix, $\mathbf{f}^{s}$ is the prescribed traction vector on the Neumann boundary Γ_f, $\mathbf{u}^{s}$ is the vector of prescribed displacements on the Dirichlet boundary Γ_u (note that the domain boundary $\Gamma = \Gamma_f \cup \Gamma_u$), $\mathbf{f}^{B}$ is the body force vector (including inertia terms), ∂_{ε} is a linear gradient operator and **N** is the matrix of direction cosine components of a unit normal to the domain boundary (positive outwards). In R^2 these vectors and matrices are written as:

$$\mathbf{u} = \begin{bmatrix} u(x,y) & v(x,y) \end{bmatrix}^{T} \tag{2.15}$$

$$\boldsymbol{\varepsilon} = \begin{bmatrix} \varepsilon_{xx} & \varepsilon_{yy} & \gamma_{xy} \end{bmatrix}^{T} \tag{2.16}$$

$$\boldsymbol{\sigma} = \begin{bmatrix} \sigma_{xx} & \sigma_{yy} & \sigma_{xy} \end{bmatrix}^{T} \tag{2.17}$$

$$\mathbf{f}^{s} = \begin{bmatrix} f_x^{s}(x,y) & f_y^{s}(x,y) \end{bmatrix}^{T} \tag{2.18}$$

$$\mathbf{u}^{s} = \begin{bmatrix} u^{s}(x,y) & v^{s}(x,y) \end{bmatrix}^{T} \tag{2.19}$$

$$\partial_{\varepsilon} = \begin{bmatrix} \partial/\partial x & 0 \\ 0 & \partial/\partial y \\ \partial/\partial y & \partial/\partial x \end{bmatrix} \tag{2.20}$$

$$\mathbf{N} = \begin{bmatrix} n_x & 0 & n_y \\ 0 & n_y & n_x \end{bmatrix} \tag{2.21}$$

$$\mathbf{C} = \begin{bmatrix} c_{11} & c_{12} & 0 \\ c_{12} & c_{11} & 0 \\ 0 & 0 & c_{33} \end{bmatrix} \qquad [2.22]$$

where for plain strain conditions

$$c_{11} = \frac{E(1-\upsilon)}{(1+\upsilon)(1-2\upsilon)},\ c_{12} = \frac{E\upsilon}{(1+\upsilon)(1-2\upsilon)},\ c_{33} = \frac{E}{2(1+\upsilon)}$$

and E and υ are the Young's modulus and Poison's ratio, respectively.

For the displacement field we have the following approximation:

$$\mathbf{u}(x,y) \simeq \sum_{J=1}^{N} \sum_{n=\zeta} \mathbf{H}_{Jn}(x,y)\boldsymbol{\alpha}_{Jn} = \mathbf{H}(x,y)\mathbf{U} \qquad [2.23]$$

where $\mathbf{U} = \begin{bmatrix} \alpha_{10} & \alpha_{11} & \alpha_{12} & \ldots & \alpha_{Jn} & \ldots \end{bmatrix}^T$ is the vector of nodal unknowns and $\boldsymbol{\alpha}_{Jn} = \begin{bmatrix} u^{Jn} & v^{Jn} \end{bmatrix}^T$ is the vector of nodal unknowns at node 'J' corresponding to the nth degree of freedom. It should be noted that unlike finite element methods, the vector of nodal unknowns is not the vector of degrees of freedom at the nodes.

Corresponding to node 'J' and nth degree of freedom, the nodal shape function matrix is

$$\mathbf{H}_{Jn}(x,y) = \begin{bmatrix} h_{Jn}(x,y) & 0 \\ 0 & h_{Jn}(x,y) \end{bmatrix} \qquad [2.24]$$

and the strain-displacement matrix is

$$\mathbf{B}_{Jn}(x,y) = \begin{bmatrix} \partial h_{Jn}/\partial x & 0 \\ 0 & \partial h_{Jn}/\partial y \\ \partial h_{Jn}/\partial y & \partial h_{Jn}/\partial x \end{bmatrix} \qquad [2.25]$$

Hence, the discretized versions of equation [2.16] and [2.17] are

$$\boldsymbol{\varepsilon}(x,y) \simeq \sum_{J=1}^{N} \sum_{n=\zeta} \mathbf{B}_{Jn}(x,y)\boldsymbol{\alpha}_{Jn} = \mathbf{B}(x,y)\mathbf{U} \qquad [2.26]$$

$$\boldsymbol{\sigma}(x,y) \simeq \sum_{J=1}^{N} \sum_{n=\zeta} \mathbf{C}\mathbf{B}_{Jn}(x,y)\boldsymbol{\alpha}_{Jn} = \mathbf{C}\mathbf{B}(x,y)\mathbf{U} \qquad [2.27]$$

The potential energy functional of the system (Bathe, 1996) is defined as

$$\pi = \frac{1}{2}\int_{\Omega} \boldsymbol{\varepsilon}^{\mathbf{T}}\boldsymbol{\sigma}\, d\Omega - \int_{\Omega} \mathbf{u}^{\mathbf{T}}\mathbf{f}^{B} d\Omega - \int_{\Gamma_f} \mathbf{u}^{\mathbf{T}}\mathbf{f}^{S} d\Gamma - \Im \qquad [2.28]$$

where $\Im$ represents the potential energy contribution from the Dirichlet boundary.

Unlike the finite element methods, the shape functions [2.6] used in the method of finite spheres do not satisfy the Kronecker of delta property at the nodes. Three techniques are predominately used to enforce the Dirichlet boundary condition: Lagrange multipliers, penalty formulation, and replacement of Lagrange multipliers with their physical significance. The third technique is described in detail in (De *et al.*, 2001). The use of Lagrange multipliers requires attention to be paid to the stability of the numerical solution. In this work we use the penalty formulation to enforce the Dirichlet boundary conditions. Hence

$$\Im = \frac{\gamma}{2}\int_{\Gamma_u} \left(\mathbf{u} - \mathbf{u}^{\mathbf{s}}\right)^{T} \left(\mathbf{u} - \mathbf{u}^{\mathbf{s}}\right) d\Gamma \qquad [2.29]$$

where γ is the penalty parameter.

Minimizing the potential energy functional in [2.28] with respect to the nodal variables results in the following set of discrete equations:

$$\mathbf{KU} = \mathbf{F} \qquad [2.30]$$

where

$$\mathbf{K} = \int_{\Omega} \mathbf{B}^{\mathbf{T}}\mathbf{C}\mathbf{B} d\Omega - \gamma\int_{\Gamma_u} \mathbf{H}^{\mathbf{T}}\mathbf{H} d\Gamma \qquad [2.31]$$

and

$$\mathbf{F} = \int_{\Omega} \mathbf{H}^{\mathbf{T}}\mathbf{f}^{B} d\Omega + \int_{\Gamma^f} \mathbf{H}^{\mathbf{T}}\mathbf{f}^{s} d\Gamma - \gamma\int_{\Gamma^u} \mathbf{H}^{\mathbf{T}}\mathbf{u}^{s} d\Gamma\,. \qquad [2.32]$$

The discretized equilibrium equations for each node '*I* 'may be written as:

$$\sum_{J=1}^{N}\sum_{n\in\zeta} \mathbf{K}_{\mathrm{Im\,Jn}}\boldsymbol{\alpha}_{\mathrm{Jn}} = \mathbf{f}_{\mathrm{Im}} \qquad [2.33]$$

where

$$\mathbf{K}_{\mathrm{ImJn}} = \int_{\Omega_I} \mathbf{B}_{\mathrm{Im}}^{T}\mathbf{C}\mathbf{B}_{\mathrm{Jn}} d\Omega - \gamma\int_{\Gamma_I^u} \mathbf{H}_{\mathrm{Im}}^{T}\mathbf{H}_{\mathrm{Jn}} d\Gamma \qquad [2.34]$$

$$\mathbf{f}_{\text{Im}} = \int_{\Omega_I} \mathbf{H}_{\text{Im}}^T \mathbf{f}^B d\Omega + \int_{\Gamma_I^f} \mathbf{H}_{\text{Im}}^T \mathbf{f}^s d\Gamma - \gamma \int_{\Gamma_I^u} \mathbf{H}_{\text{Im}}^T \mathbf{u}^s d\Gamma \quad [2.35]$$

The above integrals are evaluated using numerical integration techniques. In the finite element methods the integrands are polynomial or mapped polynomial functions defined on n-dimensional cubes or tetrahedra. Hence, efficient Gauss-Legendre product rules are used (Bathe, 1996). In the method of finite spheres, however, the integrands are non-polynomial rational functions and the integration domains are much more complex. Hence specialized integration techniques, based on piece-wise midpoint quadrature, have been developed (De *et al.*, 2001; Macri *et al*., 2004).

2.3. Generation of finite spheres for arbitrary domains in $\mathbf{R}^2$

The discussion on the method of finite spheres will not be complete without a brief mention of the techniques of generating the nodal points and the spheres on domains of arbitrary geometry. This preprocessing stage is important since inefficient node generation techniques result in higher overall solution times. We have developed an efficient technique in (Macri *et al.*, 2003) based on hierarchical partitioning of space using a data structure known as an ‘octree’ in 3D and ‘quadtree’ in 2D (Samet, 1990).

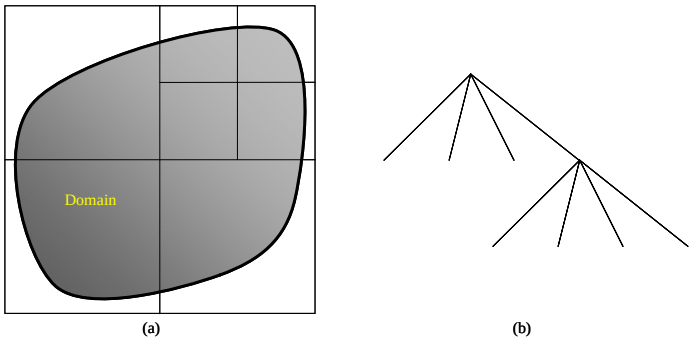

Figure 3. *In the quadtree method of generating an open cover the computational domain is first enclosed in a square box (a) which is recursively subdivided. (b) The corresponding data representation*

An example of a quadtree and its data structure is given in (figure 3a) and (figure 3b), respectively. In this technique the domain is enclosed in a square box, called a root quadrant, which is recursively subdivided into four quadrants by bisection in both Cartesian directions. The use of one-level adjusted quadtrees and face neighbor points allows neighbor search in constant time.

The placement of nodes at the centroids of the leaf quadrants with properly defined spheres centered at them automatically ensures that (1) the entire computational domain is covered by the union of the spheres; (2) all the nodal points are within the domain and (3) at any given point of the domain the number of overlapping spheres is bounded and is usually small resulting in smaller bandwidth of the resulting system matrix.

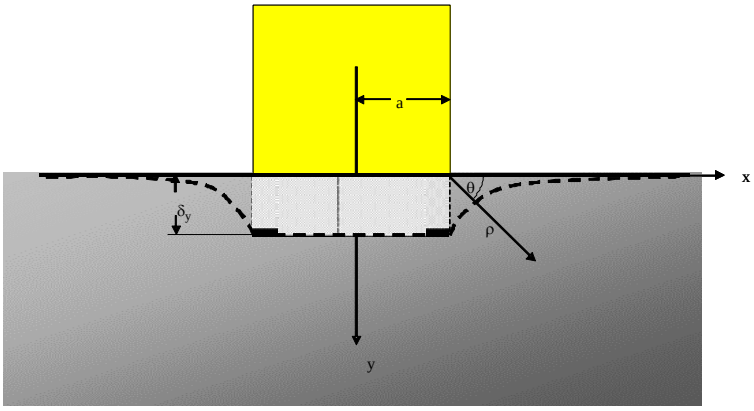

Figure 4. *An elastic half-space indented by a flat rigid punch of width '2a'*

3. Indentation of an elastic half space by a square sided rigid flat punch

In this section we consider the problem of a square sided rigid flat punch of half width '*a*' indented into an elastic half-space by δ_y (see figure 4). As in (Johnson, 1985) we restrict our problem to a punch that does not tilt, and since the punch is rigid, the following Dirichlet boundary condition is assumed

$$v^s(x,0) = \delta_y \quad -a \le x \le a \qquad [3.1]$$

The boundary condition for the x-component of the displacement field is dependent on the frictional conditions under the punch. In this paper we confine ourselves to the following two cases:

1. ***Frictionless***: the tangential component of the traction $f^t(x,0) = 0$ $-a \le x \le a$ **.**

2. ***No slip***: $u^s(x,0) = 0$ $-a \le x \le a$.

Abrupt change of boundary conditions at the edges of the punch leads to stress singularities which are difficult to capture using traditional finite element methods without excessive refinement. We will show how to generate enriched approximation schemes in the context of the method of finite spheres, by closely observing the asymptotic stress solutions, which overcome this difficulty.

3.1. *Frictionless punch*

In the frictionless case the tangential traction under the punch is zero. This solution corresponds to the case in which the interface is well lubricated. The contact pressure distribution is given as (Johnson, 1985).

$$p(x) = \frac{P}{\pi\left(a^2 - x^2\right)^{1/2}} \quad -a \le x \le a \qquad [3.2]$$

where $P = \int_{-a}^{a} p(x)dx$ is the normal force applied to the punch.

Defining $\rho = \sqrt{(x-a)^2 + y^2}$ to be the distance of the right corner of the punch (a, 0) to any point (x, y) in the domain (Figure 4) and expanding by the binomial theorem it is straightforward to show that

$$p(x) \sim \frac{1}{\sqrt{\rho}} \qquad [3.3]$$

The corresponding Muskhelishvili potential is given by

$$\Phi(z) = \frac{K^*}{2\sqrt{\rho}}\, e^{-i\theta/2}, \qquad [3.4]$$

where $\theta = \tan^{-1}\left(\frac{y}{x-a}\right)$, K^* is a stress intensity factor and $z = \rho e^{i\theta} = (x-a) + iy$ with $i = \sqrt{-1}$.

The asymptotic stress field can be derived from this potential (Sackfield *et al.*, 2003) as

$$\begin{aligned}
\sigma_{xx} &\sim \frac{K^*}{8\sqrt{\rho}}\left[3\sin\left(\frac{\theta}{2}\right) + \sin\left(\frac{5\theta}{2}\right)\right] \\
\sigma_{yy} &\sim \frac{K^*}{8\sqrt{\rho}}\left[5\sin\left(\frac{\theta}{2}\right) - \sin\left(\frac{5\theta}{2}\right)\right] \\
\sigma_{xy} &\sim -\frac{K^*}{8\sqrt{\rho}}\left[\cos\left(\frac{5\theta}{2}\right) - \cos\left(\frac{\theta}{2}\right)\right]
\end{aligned} \qquad [3.5]$$

At the surface of the elastic solid (3.5) reduces to

$$\sigma_{xx} = \sigma_{yy} = \begin{cases} \dfrac{K^*}{2\sqrt{\rho}} & \text{x} \le \text{a} \\ 0 & \text{x>a} \end{cases} \qquad [3.6]$$

$$\sigma_{xy} = 0 \qquad [3.7]$$

In figure 5 we plot the asymptotic solution for σ_{yy} for several values of *y*. An important observation is that, on the surface, $\sigma_{yy} \sim 1/\sqrt{\rho}$ as $x \to a^-$ but $\sigma_{yy} = 0$ for $|x| > a$. Hence, even though the stress field exhibits a $1/\sqrt{\rho}$ singularity, reminiscent of crack tip fields, quarter point elements cannot be used to solve this problem efficiently. Due to the same reason, we cannot simply enrich the method of finite spheres basis by including the function $\sqrt{\rho}$. Hence specialized enrichment functions are necessary.

The specific questions that we ask at this point are [1] what is the simplest enrichment function that must be used and [2] does this enrichment apply to both the x- and y-components of the displacement field? Use of complex enrichment functions is computationally inefficient since it not only leads to a larger stiffness matrix, but also results in numerical integration problems. The answer to the second question is crucial since, as we will see shortly, blindly enriching both the displacement components will result in computed stress fields that have incorrect asymptotic behavior close to the punch corner.

Based on the asymptotic solution in [3.5] we propose to use the following enrichment function

$$\sqrt{\rho}\sin\left(\frac{\theta}{2}\right) \qquad [3.8]$$

Hence, the enriched component of the shape function at node '*I*' is

$$h_I^{en} = \phi_I^0 \sqrt{\rho}\sin\left(\frac{\theta}{2}\right) \qquad [3.9]$$

whose x- and y-derivatives are, respectively,

$$h_{I,x}^{en} = \frac{1}{2\sqrt{\rho}}\sin\left(\frac{\theta}{2}\right)\left(2\phi_{I,x}^0\rho - \phi_I^0\right) \qquad [3.10]$$

$$h_{I\ ,y}^{en} = \frac{1}{2\sqrt{\rho}}\left(\phi_I^0 \cos\left(\frac{\theta}{2}\right) + 2\phi_{I,y}^0 \rho \sin\left(\frac{\theta}{2}\right)\right) \qquad [3.11]$$

where the ',' notation is used to indicate derivatives.

If we enrich both the x- and y-components of the displacement field, then the enriched part of all three components of the stress field are

$$\left\{\sigma_{xx}^{\ en}, \sigma_{yy}^{\ en}, \sigma_{xy}^{\ en}\right\} \in \frac{1}{\sqrt{\rho}} span\left\{\phi_{I,x}^{\ 0}\rho\sin\left(\frac{\theta}{2}\right), \phi_I^0 \sin\left(\frac{\theta}{2}\right), \phi_I^0 \cos\left(\frac{\theta}{2}\right), \phi_{I,y}^0 \rho \sin\left(\frac{\theta}{2}\right)\right\} \qquad [3.12]$$

which implies the following incorrect behavior

$$\left\{\sigma_{xx}^{\ en}, \sigma_{yy}^{\ en}, \sigma_{xy}^{\ en}\right\} \in \frac{1}{\sqrt{\rho}} span\left\{\phi_I^0 \sin\left(\frac{\theta}{2}\right), \phi_I^0 \cos\left(\frac{\theta}{2}\right)\right\} \text{ as } \rho \to 0 \qquad [3.13]$$

The presence of both $\sin(\theta/2)$ and $\cos(\theta/2)$ in the asymptotic solution implies that $\sigma_{yy} \sim 1/\sqrt{\rho}$ as $x \to a^-$ as well as $x \to a^+$, for instance.

From this analysis it is clear that both x- and y-components of the displacement fields should not be enriched and that one needs to enrich only the **x-component** of the displacement field to obtain the following enriched stress fields:

$$\begin{aligned} \sigma_{xx}^{en} &\propto \frac{1}{\sqrt{\rho}}\sin\left(\frac{\theta}{2}\right)\left(2\phi_{I,x}^0 \rho - \phi_I^0\right) \\ \sigma_{yy}^{en} &\propto \frac{1}{\sqrt{\rho}}\sin\left(\frac{\theta}{2}\right)\left(2\phi_{I,x}^{\ 0} \rho - \phi_I^0\right) \end{aligned} \qquad [3.14]$$

which exhibit the correct asymptotic behavior as in equation [3.5].

In the numerical solution scheme, one needs to enrich only nodes in the immediate vicinity of the punch tip where the asymptotic solution holds (figure 5). Actually, we will enrich only the node at the punch tip (figure 6) and show how this improves the overall solution.

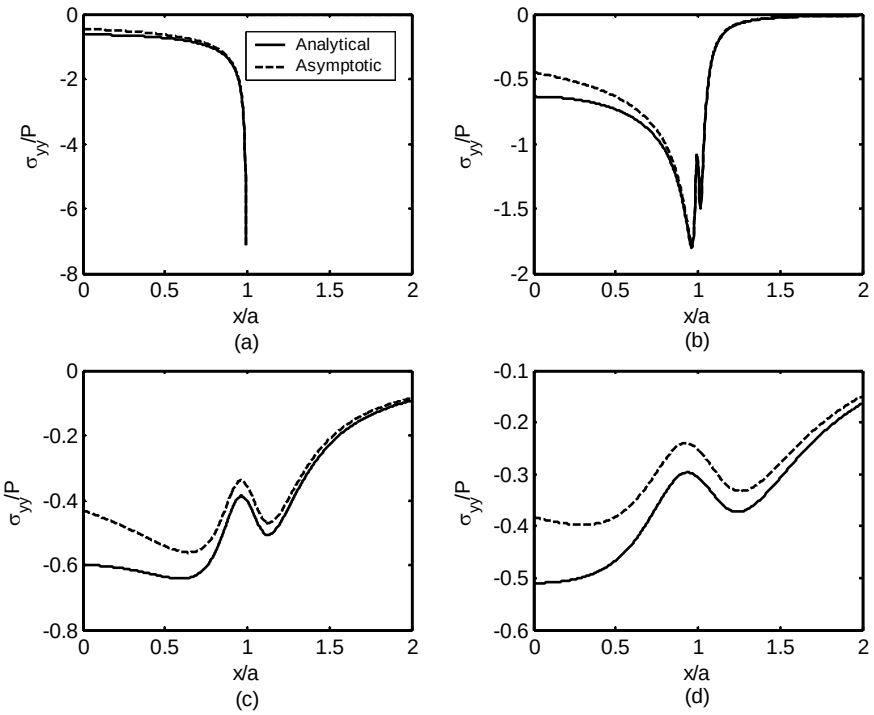

Figure 5. *The asymptotic and analytical normal stresses at (a) y = 0, (b) y = 0.01, (c) y = 0.1 and (d) y = 0.2, for a frictionless rigid punch indenting a half-space*

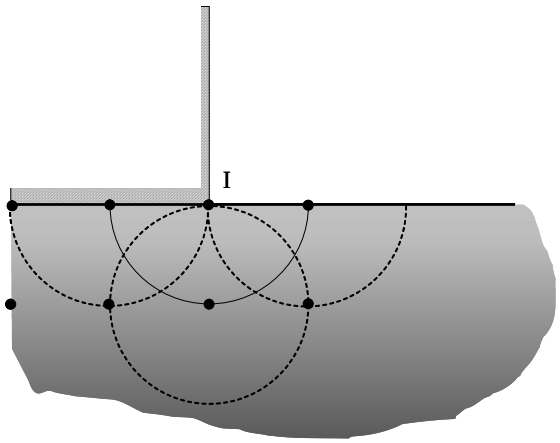

Figure 6. *MFS nodes placed around the corner of the punch. Node I, located right at the punch tip, is enriched*

3.1. *No slip case*

In this case the friction is significant to prevent any motion in the tangential direction, *i.e.* $u^s(x,0) = 0$ -a ≤ x ≤ a . The pressure distribution on the surface is given as (Johnson, 1985)

$$p(x) = \frac{2(1-\upsilon)}{(3-4\upsilon)^{1/2}} \frac{P}{\pi\left(a^2 - x^2\right)^{1/2}} \cos\left\{\eta \ln\left(\frac{a+x}{a-x}\right)\right\} \qquad [3.15]$$

where

$$\eta = (1/2\pi)\ln(3-4\upsilon) \qquad [3.16]$$

The stress singularity at the edges of the punch is oscillatory and it has been hypothesized in (Johnson, 1985) that this behavior is spurious and is due to the inadequacy of the linear elastic theory to handle high strain gradients in these regions. Another point to notice is that, unlike in the previous case, the tangential traction is nonzero and has a singularity at the punch edges.

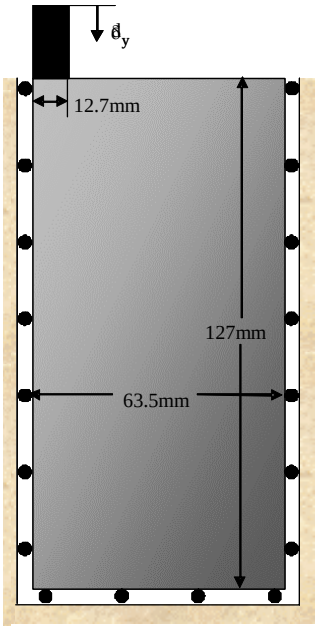

Figure 7. *A square 127mm × 127mm elastic block is indenting by δ_y with an indenter of width 25.4mm. The Young's modulus and Poisson's ratio of the block are chosen as 6.895×10^7 kPa and 0.33, respectively. Half of the problem domain is shown*

4. Numerical results

We now examine a specific problem shown in figure 7 of a square 127 mm × 127mm elastic block in plane strain, constrained along its two sides and bottom surface as shown in the figure and indented by a square-sided rigid flat punch of width 25.4mm by an amount δ_y = 2.54mm. The Young's modulus and Poisson's ratio of the block are chosen as 6.895×10^7 kPa and 0.33, respectively. This problem is solved, for both the frictionless and no slip cases, using the following three techniques: (1) traditional finite elements (a uniform mesh of nine noded quadratic elements are used and the solution is performed using the ABAQUS version 6.4 computer program), (2) the method of finite spheres (MFS) with quadratic basis and no enrichment and (3) the MFS with quadratic basis and only the node at the corner of the punch enriched with the function discussed in the previous section.

We discuss the solutions for the frictionless case in section 4.1 and the no slip case in section 4.2. In the absence of an analytical solution of the problem, we will compare the results with a solution using a very fine finite element mesh (~200,000 nodes) of nine noded elements, which we will refer to as the '**fine mesh solution**'. Mesh gradation is not employed in any of the analyses.

In the next two sections we will show that, even for considerably coarse discretizations using 5 and 9 nodes under the punch, the MFS without enrichment provides a much better solution than traditional FEM due to the considerably smooth approximation spaces used. The MFS with enrichment is capable of capturing the singularity at the corner of the punch exactly, irrespective of the discretization resolution. None of the other two schemes share this outstanding property.

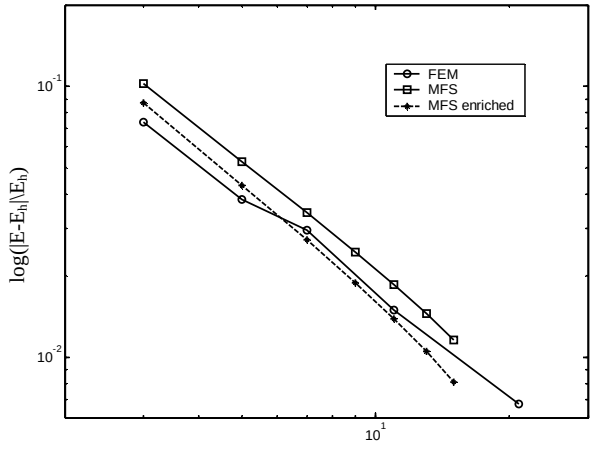

Figure 8. *The relative error in strain energy plotted as a function of number of nodes under the punch for the frictionless case. The strain energy of the mathematical model is* E *= 422.0155 J*

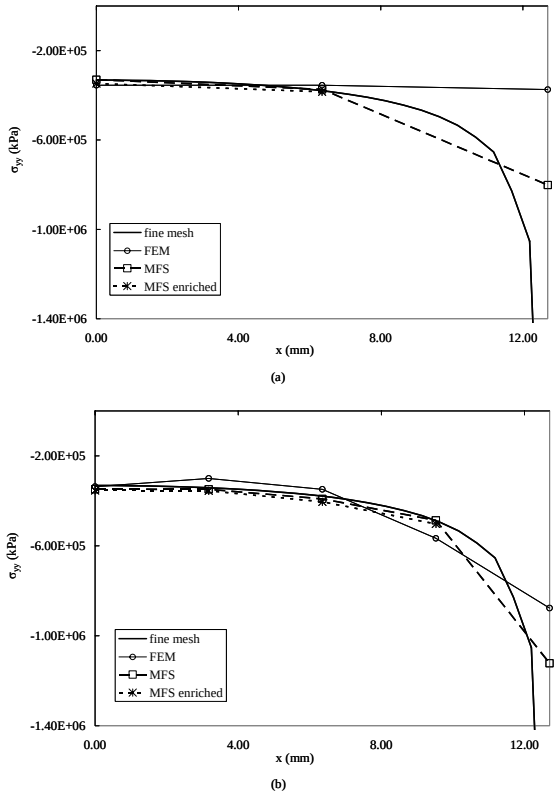

Figure 9. *For the frictionless punch example, the normal stress* $\sigma_{yy}(x,0)$ *is plotted from* $0 \le x \le 12.7$ *mm for (a) 5 nodes and (b) 9 nodes under the punch. The "fine mesh solution" is the FEM solution obtained using ~150 nodes under the punch. At the enriched MFS node, at x = 12.7mm,* $\sigma_{yy} \to -\infty$ *and therefore it has not been shown in the figure*

4.1. *Frictionless punch*

In figure 8, we compare the relative error in the strain energy as a function of the number of nodes under the punch for all three cases mentioned above. The computed strain energy is defined as

$$\mathsf{E}_h = \frac{1}{2}\int_\Omega \boldsymbol{\sigma}^T \boldsymbol{\varepsilon} d\Omega$$

where $\boldsymbol{\sigma}$ and $\boldsymbol{\varepsilon}$ are the computed stress and strain fields, respectively. The 'theoretical' strain energy of the mathematical model, E, is obtained from the fine mesh solution as 422.0155 J.

The slope of the convergence curve is 1.2305 for finite elements, 1.3469 for the method of finite spheres without enrichment and 1.4590 with enrichment. We see the enriched MFS performs marginally better than FEM in the energy norm. However, since the error in the strain energy computed in the manner described above is a global measure, we do not expect to see outstanding improvements. The real advantage of using MFS is realized by looking at the computed stress fields on the surface of the elastic block in the vicinity of the punch tip.

In figures 9a and 9b we compare σ_{yy} on the surface using 5 and 9 nodes under half the punch, respectively. We see from these plots that pure MFS predicts the stresses with higher accuracy than FEM. The solution using the enriched displacement field reproduces the singularity at the tip exactly.

In figure 10 we compare the contours of σ_{yy} in the right half of the problem domain using 5 and 9 nodes under the punch, respectively. For the solution using enriched MFS, the stress computed at the punch corners is actually infinite, and is therefore removed from this plot.

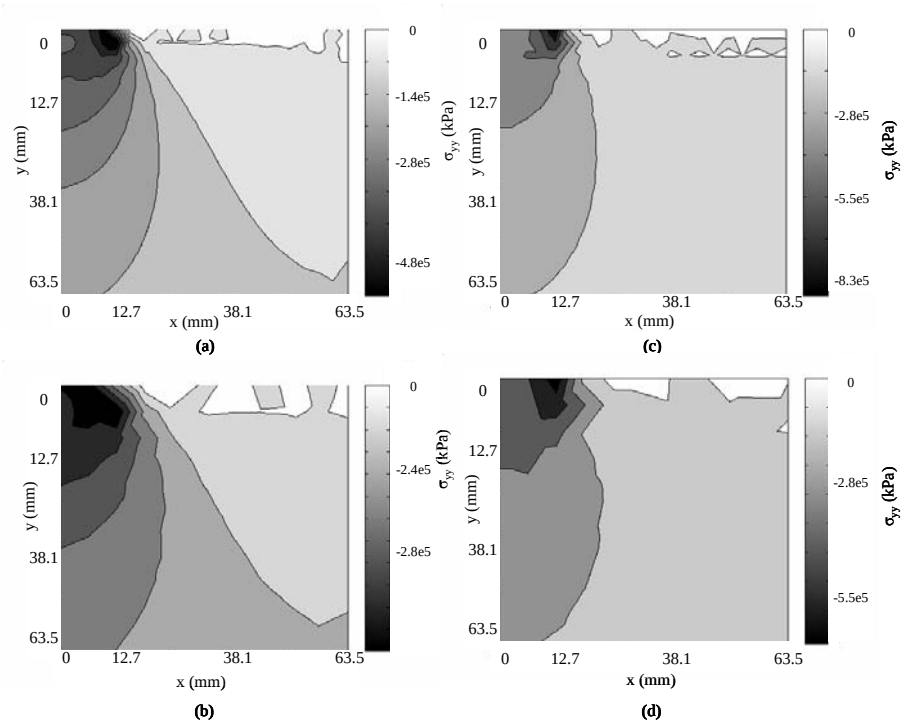

Figure 10. *Contour plots of the normal stresses σ_{yy} (kPa) in the right half of the problem for the frictionless case. (a) and (b) correspond to solution obtained using enriched MFS with 9 and 5 nodes respectively, excluding the singularity at the corner. (c) and (d) correspond to solutions obtained using FEM with 9 and 5 nodes respectively*

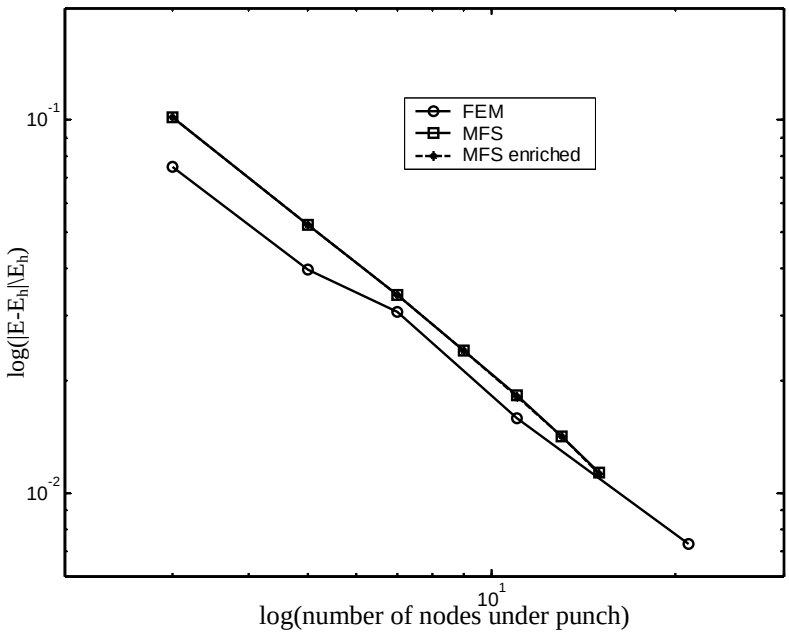

Figure 11. *The relative error in strain energy plotted as a function of number of nodes under the punch for the no slip case. The strain energy of the mathematical model is* E *= 428.2564 J*

4.2. *No slip case*

For the no slip case, we examine the error in strain energy verses the number of nodes under the punch in figure 11. The slopes of the convergence curves are 1.1960 for FEM, 1.3567 for MFS and 1.3574 for enriched MFS. As in the previous case, the use of MFS and enriched MFS does improve overall convergence rate but not substantially.

Finally, in figure 12 (a) and (b) we plot the normal stress σ_{yy}. In both cases we observe that infinite stress are computed at the punch corner using enriched MFS which also provides much better stress solutions than FEM. In figure 13, we examine the contours of the stress σ_{yy} in the right half of the problem for 5 and 9 nodes under the punch. For the enriched MFS case we exclude the infinite value at the corner of the punch. From the figure we see that enriched MFS produces smoother results than FEM.

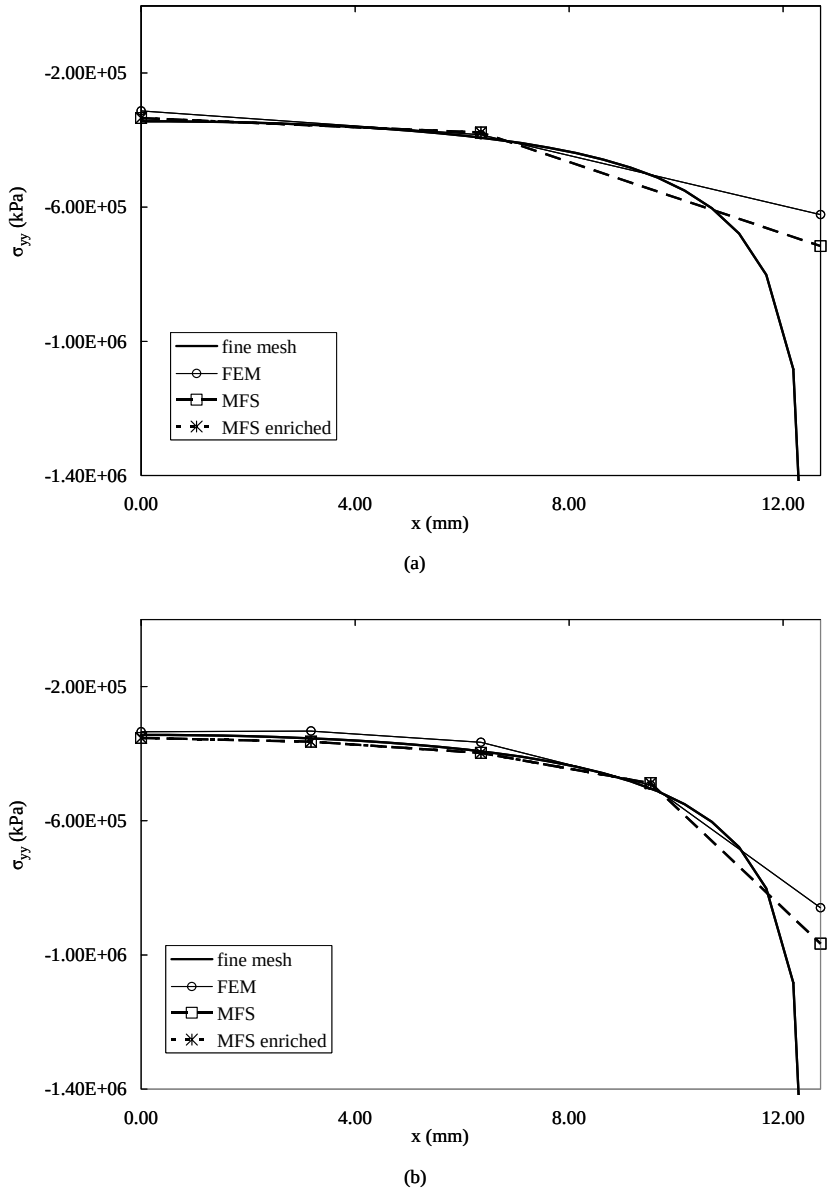

Figure 12. *For the no slip case, the normal stress,* $\sigma_{yy}(x,0)$ *is plotted from* $0 \le x \le 12.7$ *mm for (a) 5 nodes and (b) 9 nodes under the punch. The "fine mesh solution" is the FEM solution obtained using ~150 nodes under the punch. At the enriched MFS node, at x = 12.7mm,* $\sigma_{yy} \to -\infty$ *and therefore it has not been shown in the figure*

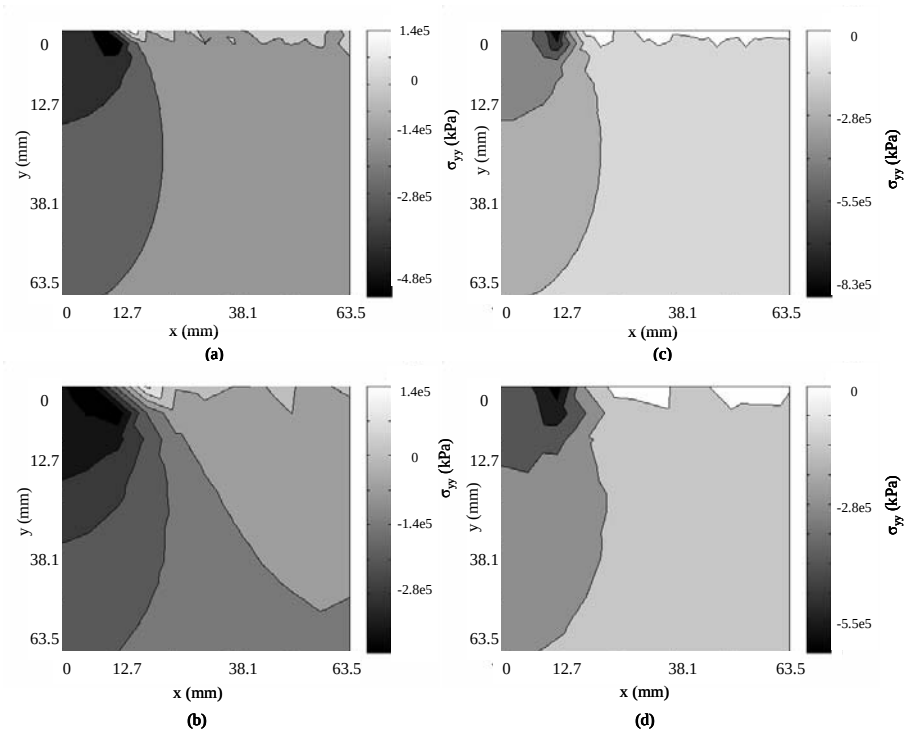

Figure 13. *Contour plots of the normal stresses (kPa) in region of punch corner for the no slip case. (a) and (b) are examples of enriched MFS with 9 and 5 nodes respectively, excluding the singularity at the corner. (c) and (d) are examples of FEM with 9 and 5 nodes respectively*

5. Conclusions

In this paper we have presented the method of finite sphere as a promising numerical technique for the solution of problems arising in tribology. Not only is it a truly meshfree method where interpolation and numerical integration may be performed without a mesh, but it also provides a very powerful and general route to generating approximations which can be tailored to exploit the structure of the solution of the governing differential equation. An example of a square-edged flat punch indenting an elastic block has been used to showcase these features.

While the current paper presents a purely displacement-based formulation, for problems involving incompressible or nearly incompressible deformations displacement-pressure mixed formulations have been developed for the method of finite spheres which are stable and reliable (De *et al.*, 2001).

For the flat punch problem only two situations have been discussed: one corresponding to a frictionless interface and the other dealing with a no slip interface. For a more general situation of partial slip one needs to develop and employ a contact algorithm to capture the complex stick-slip patterns. However, the same principle of enrichment presented in this paper is still applicable.

6. References

Akin J. E., "The generation of elements with singularities", *International Journal for Numerical Methods in Engineering*, Vol. 10, 1976, pp. 1249-1259.

Atluri S. N., Zhu T., "A new meshless local Petrov-Galerkin (MLPG) approach in computational mechanics", *Computational Mechanics*, Vol. 22, 1998, pp. 117-127.

Babuska I., Melenk J. M., "The partition of unity method", *International Journal for Numerical Methods in Engineering*, Vol. 40, 1997, pp. 727-758.

Baheti S. K., Kirk R. G., "Finite Element Thermo-Hydrodynamic Analysis of a Circumferentially Grooved Floating Oil Ring Seal", *STLE Tribology Transactions*, Vol. 38, 1995, pp. 86-96.

Banks-Sills L., Bortman Y., "Reappraisal of the quarter-point quadrilateral element in linear elastic fracture mechanics", *International Journal of Fracture*, Vol. 25, 1984, pp. 169-180.

Barsoum R. P. "Triangular quarter-point elements as elastic ad perfectly-plastic crack tip elements", *International Journal for Numerical Methods in Engineering*, Vol. 11, 1984, pp. 185-198.

Bathe K. J., *Finite Element Procedures*, Englewood Cliffs, NJ, Prentice-Hall, 1996.

Belytschko T., Lu Y. Y., Gu L., "Element free Galerkin methods", *International Journal for Numerical Methods in Engineering*, Vol. 37, 1994, pp. 229-256.

De S., Bathe K. J., "The method of finite spheres with improved numerical integration", *Computers & Structures*, Vol. 79, 2001, pp. 2183-2196.

De S., Bathe K. J., "Displacement/pressure mixed interpolation in the method of finite spheres", *International Journal for Numerical Methods in Engineering*, Vol. 51, 2001, pp. 275-292.

Duarte C. A., Oden, J. T., "H-p clouds – an hp meshless method", *Numerical Methods for Partial Differential Equations*, Vol. 12, 1996, pp. 673-705.

Geijselaers H. J. M., Koning A. J. E., "Finite Element Analysis of Thermoelastic Instability with Intermittent Contact", *ASME Journal of Tribology*, Vol. 122, 2000, pp. 42-46.

Jacq C., Nélias D., Lormand G., Girodin D., "Development of a Three-Dimensional Semi-Analytical Elastic-Plastic Contact Zone", *ASME Journal of Tribology*, Vol. 124, 2002, pp. 653-367.

Johnson K. L., *Contact Mechanics, Cambridge*, UK, Cambridge University Press,1985.

Kim A. T., Seok J., Tichy J. A., Cale T. S., "Multiscale Elastohydrodynamic Contact Model for CMP", *Journal of the Electrochemical Society*, Vol. 150, 2003, pp. G570-G576.

Komvopoulos K., Ye N., "Elastic-Plastic Finite Element Analysis for the Head-Disk Interface with Fractal Topography Description", *ASME Journal of Tribology*, Vol. 124, 2002, pp. 775-784.

Li S., Liu W. K., "Moving least-square reproducing kernel methods, part II: Fourier analysis", *Computer Methods in Applied Mechanics and Engineering*, Vol. 139, 1996, pp. 159-193.

Li S., Liu W. K., "Reproducing kernel hierarchical partition of unity, part I – formulation and theory", *International Journal for Numerical Methods in Engineering*, Vol. 45, 1999, pp. 251-288.

Liu W. K., Adee J., Jun S., "Reproducing kernel particle methods for elastic and plastic problems", In: Benson D. J., Asaro R. A. (eds) *Advanced Computational Methods for Material Modeling, AMD 180 and PVP 33*, ASME 1993, pp. 175-190.

Macri M., De S., Shephard M. S., "Hierarchical tree-based discretization for the method of finite spheres", *Computers & Structures*, Vol. 81, 2003, pp. 789-803.

Macri M., De S., "Towards an automatic discretization scheme for the method of finite spheres and its coupling with the finite element method", *Computers & Structures*, 2004 (in press).

Melenk J. M., Babuska I., "The partition of unity finite element method: basic theory and applications", *Computer Methods in Applied Mechanics and Engineering*, Vol. 139, 1996, pp. 289-314.

Monaghan J. J., "An introduction to SPH", *Computer Physics Communications*, Vol. 48, 1988, pp. 89-96.

Nayroles B., Touzot G., Villon P., "Generalizing the FEM: diffuse approximation and diffuse elements", *Computational Mechanics*, Vol. 10, 1992, pp. 307-318.

Onate E., Idelsohn S., Zienkiewicz O. C., "A finite point method in computational mechanics, applications to convective transport and fluid flow", *International Journal for Numerical Methods in Engineering*, Vol. 39, 1996, pp. 3839-3866.

Optasanu V., Bonneau D., "Finite Element Mass-Conserving Cavitation Algorithm in Pure Squeeze Motion. Validation to a Connecting Rod Small End Bearing", *ASME Journal of Tribology*, Vol. 122, 2000, pp. 162-169.

Ruan B., "Finite Element Analysis of the Spiral Groove Face Seal at the Slow Speed and the Low Pressure Conditions – Slip Flow Consideration", *STLE Tribology Transactions*, Vol. 43, 2000, pp. 411-418.

Sackfield A., Mugadu A., Barber J. R., Hills D. A., "The application of asymptotic solutions to characterizing the process one in almost complete frictionless contacts", *Journal of the Mechanics and Physics of Solids*, Vol. 51, 2003, pp. 1333-1346.

Samet H., *The design and analysis of spatial data structures*, Addison-Wesley Publishing Company, Inc., 1990.

Shepard D., “A two-dimensional interpolation function for irregularly spaced data”, *Proc 23rd National Conference ACM*, 1968, pp. 517-524.

Stephens L. S., Liu Y., Meletis E. I., “Finite Element Analysis of the Initial Yielding Behavior of a Hard Coating/Substrate System with Functionally Graded Interface under Indentation and Friction”, *ASME Journal of Tribology*, Vol. 122, 2000, pp. 381-387.

Xu B., Jiang Y., “Elastic-Plastic Finite Element Analysis of Partial Slip Rolling Contact”, *ASME Journal of Tribology*, Vol. 124, 2002, pp. 20-26.

Zhu T., Zhang J. D., Atluri S. N., “A local boundary integral equation (LBIE) method in computational mechanics and a meshless discretization approach”, *Computational Mechanics*, Vol. 21, 1998, pp. 223-235.